Pipe drift estimation based on the measurements of geometrical parameters from a single pipe

Luca Bellani

Aramis s.r.l., Milano, Italy. E-mail: luca.bellani@aramis3d.com

Michele Compare

Aramis s.r.l., Milano, Italy. E-mail: michele.compare@aramis3d.com
Energy Department, Politecnico di Milano, Italy

Enrico Zio

Energy Department, Politecnico di Milano, Italy. E-mail: enrico.zio@polimi.it
Aramis s.r.l., Milano, Italy
MINES ParisTech, PSL Research University, CRC, Sophia Antipolis, France
Eminent Scholar, Department of Nuclear Engineering, College of Engineering, Kyung Hee University,
Republic of Korea

Gustavo Almeida, Pedro Filgueiras

Vallourec R&D, Rio de Janeiro, Brasil. E-mail: g.almeida@vallourec.com; pedro.filgueiras@vallourec.com

Pipe drift is among the most relevant quality factors of pipes for deep water applications. This is estimated through empirical models encoding geometrical parameters. In a previous work, we relied on Gaussian fields to map these parameters onto the pipe drift conformance probability. The field kernel was estimated from a set of measurements gathered from pipes of the same lot, produced at the same mill. However, in practice it is very difficult to find this homogeneous dataset. The objective of this paper is to extend the previously developed framework to estimate the drift based on the geometrical data relevant to a single pipe, only. For this, we consider known analytical kernels and infer their parameters from the single pipe measurements. Then, we estimate the actual error on the drift conformance probability estimations, considering the best fitting kernel. This error turns out to be negligible.

Keywords: Pipe drift, Gaussian Field, Single Pipe.

1. Introduction

The drift of a pipe is a measure of the roundness of its inside wall. When the drift is out of specification, tools, pumps, smaller pipes and other items are no longer guaranteed to pass through the pipe. In Oil&Gas deep water applications, this leads to major consequences on the well operability and, thus, on its economic performances. Given the relevance of drift, pipes not meeting the acceptance requirement are discarded. This improves the quality of the purchased pipes, but strongly affects their production costs, in an Oil&Gas industry context where currently there is a urgent need for cost reduction Crooks (2016); Hovem (2019).

Pipe drift can be estimated through empirical models encoding geometrical parameters such as pipe diameters and thickness, which are accurately measured at discrete points on every produced pipe. This measurement-based approach, however, ensures that the drift requirement is met over the entire pipe, only if we assume that the geometrical parameters are not diverging between two successive measurement points. This assumption cannot be straightforwardly accepted.

To overcome this issue, a novel framework is proposed in Pinciroli et al. (2019) to estimate the drift conformance probability (i.e., probability of having drift values meeting the requirements over the entire pipe ISO/IEC-GUIDE:98-4 (2012)). This is based on the Gaussian field theory, where the Gaussian field kernel is inferred from a homogeneous dataset of pipe geometrical parameters, measured from pipes of the same type and produced at the same mill. The drift conformance probability of each pipe is a posteriori estimated through a Bayesian updating of the field, based on the gathered evidence of the measurements. In particular, the framework proposed in Pinciroli et al. (2019) adopts a numerical approach for kernel estimation, which infers from the available

dataset the entries of the covariance matrix among the measumerent points, with no assumption on the kernel shape.

The approach proposed in Pinciroli et al. (2019) is limiting in practice, as it is very difficult to find homogeneous datasets to estimate the kernel. In fact, Oil&Gas mills produce pipes of different families, each requiring significant changes in the production settings that modify the kernel shapes. In this work, we extend the framework proposed in Pinciroli et al. (2019) to estimate the drift conformance probability of a single pipe, based on its measured parameters, only. In this new setting, we do not a priori know the analytical formula of the kernel; even if we did, the estimation of its parameters would rely on poor data only (i.e., those of the single pipe). Moreover, the numerical approach adopted in Pinciroli et al. (2019) for kernel estimation is not applicable, as it would use only one sample to estimate the covariance between pipe measurement points at the largest distance, only two values to estimate the covariance between measurement points at the largest but one distance, and so on.

To takle this issue, we investigate the estimation error in the drift conformance probability when we apply known analytical kernels and infer their parameters from a single pipe.

The remainder of this paper is organized as follows. In Section 2, the pipe drift model is presented. In Section 3, the developed methodology is shown. Section 4 reports the results obtained by applying the proposed methodology to a case study derived from a dataset of real pipe measurements. However, to protect the intellectual property, the original data have been all modified by applying some corrective factors. Section 5 concludes the work.

2. Pipe drift

Consider a pipe of length L mm. We assume that the available measuring sensors acquire the following geometrical parameters at pipe sections $\chi = \{\chi_1, ..., \chi_d\} \subset \Omega = [0, L] \subset \mathbb{R}$, equally spaced at a distance $\Delta = L/d$ mm:

- Average wall thickness, Wt_{av};
- Maximum wall thickness, Wt_{max};
- Average outer diameter, Od_{av};

These pipe features allow estimating the drift by means of a mathematichal model derived from API (1994); ISO/TR-10400 (2007). For confidentiality, this is not explicitly reported and, thus, it is genericaly defined as:

$$Dr =$$
$$f\left(\mathbb{E}_{l_{Dr}}[Wt_{av}], \mathbb{E}_{l_{Dr}}[Wt_{max}], \mathbb{E}_{l_{Dr}}[Od_{av}], \epsilon_{Dr}\right) \quad (1)$$

where

- ϵ_{Dr} is a vector of random variables representing the epistemic uncertainties in the drift model; these variables depend on the pipe manufacuring process and have been estimated based on a large dataset of produced pipes.
- $\mathbb{E}_{l_{Dr}}[Od_{av}]$, $\mathbb{E}_{l_{Dr}}[Wt_{av}]$ and $\mathbb{E}_{l_{Dr}}[Wt_{max}]$ represent the average values over a critical length l_{Dr} mm of the average outer diameter, average wall tickness and maximum wall tickness, respectively. In particular, the estimations of these values at pipe section χ_i consider its first $N^{Dr} = \lceil l_{Dr}/\Delta \rceil$ subsequent sections, $i = 1, ..., N_D$, $N_D = d - N^{Dr} + 1$, where $\lceil \circ \rceil$ indicates the ceiling value of its argument.

Notice that in Eq. (1) it is assumed that the smaller the value of Dr, the worsen is the pipe quality. Then, to evaluate the pipe drift conformance probability, we estimate the probability that Dr does not go below the threshold requirement T_D in any point of the pipe.

When we get the measurements of Wt_{av}, Wt_{max} and Od_{av} at points χ, we first rely on Eq. (1) to propagate the uncertain quantities ϵ_{Dr} onto the drift values, through the Monte Carlo method. Namely, at every measurement location $\chi_i \in \chi_D = \{\chi_1, ..., \chi_{N_D}\}$, we sample $N_{MC} >> 1$ (e.g., $N_{MC} = 10^7$) values from the distribution of ϵ_{Dr}. These samples enter the drift model to get the corresponding N_{MC} values of Dr, which determine the distribution of the drift assigned to the pipe section. Then, any quantile $p \in]0, 1[$ of this distribution can be considered, defining the random variable $X_p(\chi_i)$. This can be framed as the drift value at pipe section χ_i if the pipe were in the p-th portion of produced pipes leading to the worst values of ϵ_{Dr}.

To simplify the notation, we indicate by $X_{p,i}$ the variable $X_p(\chi_i)$, $i = 1, ..., N_D$. The vector of random variables $X_{p,i}$, $i = 1, ..., N$, $p \in]0, 1[$ and the corresponding values derived from the measurements of the geometrical features of the pipe are indicated by, respectively:

$$\mathbf{X}_p = [X_{p,1}, ..., X_{p,N_D}] \quad (2)$$
$$\mathbf{x}_p = [x_{p,1}, ..., x_{p,N_D}] \quad (3)$$

It is tempting to assume that if all the points of $\mathbf{X}_p$ are above T_D, then the conformance probability of the pipe is at least p. However, this definition disregard the drift in points belonging to $\Omega \setminus \chi_D$ and, thus, it provides over-estimations $\overline{\Pi}$ of the actual conformance probability Π, especially when the distance between points in χ_D is large. In

Proceedings of the 30th European Safety and Reliability Conference and
the 15th Probabilistic Safety Assessment and Management Conference

2728

formulas:

$$\Pi < \overline{\Pi} = 1 - \min_{p \in]0,1[} \left\{ p | \min_{i \in \{1,\ldots,N_D\}} X_{p,i} > T_D \right\} \tag{4}$$

Then, we need to estimate the probability that the drift goes below threshold T_D over the entire pipe.

3. Methodology

To infer the behavior of the drift in any point $\chi \in \Omega$, we assume that measurements $\mathbf{x}_p$ belong to a realization of a wide-sense stationary Gaussian random field $\mathbf{f}_p$, i.e. $\mathbf{X}_p = \mathbf{f}_p(\boldsymbol{\chi}_D)$:

- $\mathbb{E}[\mathbf{f}_p(\chi)]$ is constant for any $\chi \in \Omega$. The constant mean is indicated by $\mathbb{E}[\mathbf{f}_p(\chi)] = \mu_p$, $\forall \chi \in \Omega$, $p \in]0,1[$ and is estimated as the mean of the pipe drift over all sections, i.e.,

$$\mu_p \simeq \frac{\sum_{j=1}^{N_D} x_{p,j}}{N_D} \tag{5}$$

- The covariance function is invariant to translations, i.e., it depends on $\tau = \chi - \psi$, only Rasmussen and Williams (2018): $\gamma(\chi, \psi) = \mathbb{E}[(\mathbf{f}_p(\chi) - \mu_p)(\mathbf{f}_p(\psi) - \mu_p)] = \gamma(\tau)$, $\chi, \psi \in \Omega$.

Given that we do not know the kernel of the single pipe, we assume that it belongs to a family of kernels described by few hyper-parameters (e.g., Squared Exponential (SE), Matérn, Rational Quadratic, etc. Rasmussen and Williams (2018); Duvenaud et al. (2013)), covering a wide set of possible shapes, which are estimated through the following procedure.

Consider a set $\mathcal{K}_p = \{\gamma_{p,1}, \ldots, \gamma_{p,K}\}$ of candidate kernels, where $\gamma_{p,k}(\tau) = \gamma_{p,k}(\tau; \boldsymbol{\theta}_{p,k})$. The hyper-parameters $\boldsymbol{\theta}_{p,k}$ of each kernel $\gamma_{p,k}, k \in \{1, \ldots, K\}$, are estimated through Maximum Likelihood Estimation (MLE) on the available measurements. The likelihood reads as in Eq. 6, where $\mathbf{M}_{\mathbf{X}_p} \in \mathbb{R}^{N_D}$ is the vector containing N_D times the mean value μ_p and $\mathbf{K}_{\mathbf{X}_p} \in \mathbb{R}^{N_D} \times \mathbb{R}^{N_D}$ is the matrix whose (i,j) entry reads $\mathbf{K}_{\mathbf{X}_p}(i,j; \boldsymbol{\theta}_{p,k}) = \gamma_{p,k}(\tau = |\chi_i - \chi_j|; \boldsymbol{\theta}_{p,k})$, $i, j \in \{1, .., N_D\}$. $det \mathbf{K}_{\mathbf{X}_p}$ is the determinant of $\mathbf{K}_{\mathbf{X}_p}$, whereas $\mathbf{K}_{\mathbf{X}_p}^{-1}$ is its inverse matrix.

For each kernel $\gamma_{p,k} \in \mathcal{K}$, we find:

$$\boldsymbol{\theta}_{p,k}^{MLE} = \arg\max_{\boldsymbol{\theta}_{p,k}} L(\boldsymbol{\theta}_{p,k}) \tag{7}$$

Then, we select from the set of candidates the kernel $\gamma_p^*(\tau; \boldsymbol{\theta}_{p,k}^{MLE})$ with the smallest Akaike Information Criterion (AIC Akaike (1974)):

$$AIC_{p,k} = -2 \cdot \log L(\boldsymbol{\theta}_{p,k}^{MLE}) + 2 \cdot |\boldsymbol{\theta}_{p,k}^{MLE}| \tag{8}$$

where $|\boldsymbol{\theta}_{p,k}^{MLE}|$ is the number of hyper-parameters of the considered kernel $\gamma_{p,k}$.

Of course, other performance metrics such as the Bayesian Information Criterion (BIC) can be considered (Stone (1979)); our choice is justified by the fact that we are not sure that the proper kernel is among the set of the considered ones and, thus, the AIC metric is more suitable than BIC.

We partition the pipe through a strict grid

$$\boldsymbol{\phi}_D = \{\phi_1, \ldots, \phi_{N_Z}\} \subset \Omega \tag{9}$$

of N_Z points such that $\boldsymbol{\chi}_D \cap \boldsymbol{\phi}_D = \emptyset$ and we characterize the uncertainty in the pipe drift with the random vector $\mathbf{Z}_p = \mathbf{f}_p(\boldsymbol{\phi}_D) = [Z_{p,1}, \ldots, Z_{p,N_Z}]$. This can be done through Eq. 10, where $\mathbf{K}_{\mathbf{X}_p, \mathbf{z}_p}^*$ is the matrix whose (i,j) entry encodes the kernel γ_p^* evaluated at $\chi_i - \phi_j$, i.e., $\mathbf{K}_{\mathbf{X}_p, \mathbf{z}_p}^*|_{i,j} = \gamma_p^*(\chi_i - \phi_j)$. On this basis, we can estimate the probability that all points in $\mathbf{Z}_p$ are above the drift acceptability threshold T_D:

$$P_{N_Z,p} = \mathbb{P}\left(\min_{i \in \{1,\ldots,N_Z\}} Z_{p,i} \geq T_D\right) \tag{11}$$

This value can be interpreted as the probability that the drif of the pipe is acceptable, provided that the manufacturing process for the pipe (encoded in ϵ_{Dr}) is not worsen than that of the $1 - p$ portion of produced pipes. Certainly, for this sentence to be rigorous, we should convert the considered point-wise approach (Eqs. 9-11)) to a continuous approach. However, according to Baker and Faber (2007), no methods exist for computing this excursion probability conditional on gathered observations Adler (1981, 2000); Adler and Taylor (2007).

Notice also that an alternative approach is to consider all the kernels in $\mathcal{K}_p$, rather than only γ_p^*, and take as reliability value the smallest obtained with all kernels. This, however, makes the estimation very conservative, as kernels with large AIC value are also considered.

Finally, to set N_Z we can proceed through trial and error, by increasing its value up to when changes in the estimations of $P_{N_Z,p}$ are negligible.

4. Case study

The available dataset is composed of the measurements of minimum, average and maximum values of Wt and Od along the length of $N_T = 169$ similar pipes. For confidentiality, length L is not disclosed. The measurements are collected every Δ mm, leading to $d = 125$, $N^{Dr} = 14$ and $N_D = d - N^{Dr} + 1 = 111$.

Notice that to protect the intellectual property, the original data have been all modified by applying

$$L(\boldsymbol{\theta}_{p,k}) = f_{\mathbf{X}_p}(\mathbf{x}_p) = \frac{1}{\sqrt{(2\pi)^{N_X} det\mathbf{K}_{\mathbf{X}_p}(\boldsymbol{\theta}_{p,k})}} e^{-\frac{1}{2}(\mathbf{x}_p - \mathbf{M}_{\mathbf{X}_p})^T \mathbf{K}_{\mathbf{X}_p}(\boldsymbol{\theta}_{p,k})^{-1}(\mathbf{x}_p - \mathbf{M}_{\mathbf{X}_p})} \qquad (6)$$

$$\mathbf{Z}_p|\mathbf{X}_p; \mu_p, \gamma_p^* \sim \mathcal{N}(\mathbf{K}_{\mathbf{Z}_p}^* \mathbf{K}_{\mathbf{X}_p}^{*-1}(\mathbf{X}_p - \mathbf{M}_{\mathbf{X}_p}), \mathbf{K}_{\mathbf{Z}_p}^* - \mathbf{K}_{\mathbf{Z}_p,\mathbf{X}_p}^* \mathbf{K}_{\mathbf{X}_p}^{*-1} \mathbf{K}_{\mathbf{X}_p,\mathbf{z}_p}^*) \qquad (10)$$

some corrective factors and the value of the critical length l_{Dr} is not reported.

Now, we evaluate the reliability of the single pipes using the methodology reported in Section 3, setting $p = 0.05$, $N_Z = 2\,000$ and assuming that the decision maker will not discard the pipes if $\mathrm{P}_{N_Z,p} = \mathrm{P}_{2000,0.05} > 1 - 10^{-5}$.

Our candidate kernels are (Rasmussen and Williams (2018)):

- Matérn 1.5 kernel $\gamma_{p,1}(\tau; \boldsymbol{\theta}_{p,1}) =$

$$C \cdot \left(1 + \frac{\sqrt{3}\tau}{l}\right) \cdot e^{-\frac{\sqrt{3}\tau}{l}}$$

where $\boldsymbol{\theta}_{p,1} = [l, C]$, l is the length scale parameter and C is the noise level parameter.

- Matérn 0.5 kernel $\gamma_{p,2}(\tau; \boldsymbol{\theta}_{p,2}) =$

$$C \cdot e^{-\frac{\tau}{l}}$$

where $\boldsymbol{\theta}_{p,2} = [l, C]$, where l and C are the parameters described above.

- Periodic times Matérn 1.5 $\gamma_{p,3}(\tau; \boldsymbol{\theta}_{p,3}) =$

$$e^{-2\left(\frac{\sin\left(\frac{\pi}{P}(\tau)\right)}{l}\right)^2} \cdot \gamma_{p,1}(l, C)$$

where $\boldsymbol{\theta}_{p,3} = [P, \lambda, l, C]$, and P is the period, λ is the length scale of the periodic kernel, l is the length scale parameter and C is the noise level parameter.

- Periodic times Matérn 0.5 $\gamma_{p,4}(\tau; \boldsymbol{\theta}_{p,4}) =$

$$e^{-2\left(\frac{\sin\left(\frac{\pi}{P}(\tau)\right)}{\lambda}\right)^2} \cdot \gamma_{p,2}(l, C)$$

where $\boldsymbol{\theta}_{p,4} = [P, \lambda, l, C]$, and the parameters are the same described above.

- Periodic times Matérn 1.5 + Periodic times Matérn 0.5 $\gamma_{p,5}(\tau; \boldsymbol{\theta}_{p,5}) =$

$$\gamma_{p,3}(P_1, \lambda_1, l_1, C_1) + \gamma_{p,4}(P_2, \lambda_2, l_2, C_2)$$

where $\boldsymbol{\theta}_{p,5} = [P_1, \lambda_1, l_1, C_1, P_2, \lambda_2, l_2, C_2]$, and the parameters are the same described above.

- RBF $\gamma_{p,6}(\tau; \boldsymbol{\theta}_{p,6}) =$

$$e^{-\frac{\tau}{l}^2} \cdot C$$

where $\boldsymbol{\theta}_{p,6} = [l, C]$, l is the length scale parameter and C is the noise level parameter.

- White $\gamma_{p,7}(\tau; \boldsymbol{\theta}_{p,7}) = 0$, which denotes that there is no correlation between consecutive samples.

As reported in Rasmussen and Williams (2018), all the considered kernels are stationary, as they are sums and products of stationary kernels.

Notice that kernels with non differentiable spectra such as the Matérn 0.5 entail that there are discontinuities in the derivatives of the drift: when there is a large correlation between neighbor sections, the drift in points in $\Omega \setminus \chi_D$ may exhibit a larger variability with respect to smoother kernels Rasmussen and Williams (2018).

In Table 1, we report, for each of the candidate kernels $\gamma_{p,k} \in \mathcal{K}_p$ (first row), the portion of the N_T available pipes for which it has the smallest AIC value; that is, column k reports the portion of times $\gamma_{p,k} = \gamma_p^*$, $k \in \{1, \ldots, 7\}$. We can see that approximately 50% of times, the mixture of the two periodic kernels has the smallest AIC value. Moreover, 79% of the times a kernel with a periodic component is selected. This is due to the presence of a periodic geometry in the pipes. Finally, the Matérn 0.5, RBF and White kernels never have the smallest AIC.

Notice that the grid sections $\mathbf{Z}_p$ are uniformly

Table 1.: Percentage of pipes which have as kernel with smallest AIC kernel $\gamma_{p,k}, k \in \{1, \ldots, 7\}$.

$\gamma_{p,1}$	$\gamma_{p,2}$	$\gamma_{p,3}$	$\gamma_{p,4}$	$\gamma_{p,5}$	$\gamma_{p,6}$	$\gamma_{p,7}$
0.29	0	0.11	0.11	0.49	0	0

distributed along the pipe length. However, different approaches can be used to estimate the value of $\mathrm{P}_{N_Z,p}$ for the considered pipe (e.g., Chevalier et al. (2014); Azzimonti et al. (2016)). For instance, increasing the number of points close to sections where $\mathbf{X}_{p=0.05}$ is small is expected to provide more accurate estimations of the downcrossing probability. Further research work will

Proceedings of the 30th European Safety and Reliability Conference and
the 15th Probabilistic Safety Assessment and Management Conference

2730

tackle this issue.

Figure 1 reports the drift in all sections of the pipes; we have highlighted with different markers the pipes:

- which do not cross the threshold T_D in any of the points belonging to χ_D and have $P_{2000,0.05} > 1 - 10^{-5}$.
- which either cross the threshold T_D in any of the points belonging to χ_D or do not cross the threshold but have $P_{2000,0.05} < 1 - 10^{-5}$. These are reoported in Figure 2.

From the analysis of the Figures, we can see that there are 4 pipes out of 169 which do not satisfy the requirements on drift (Figure 2). Among these, two pipes have a drift undergoing threshold T_D at some measurements sections, whereas the other two have a probability of down-crossing the threshold larger than -10^{-5}, even if the drift is acceptable at points in Section χ_D. Notice that these two pipes are the closest to the threshold T_D, especially at χ_D close to 100.

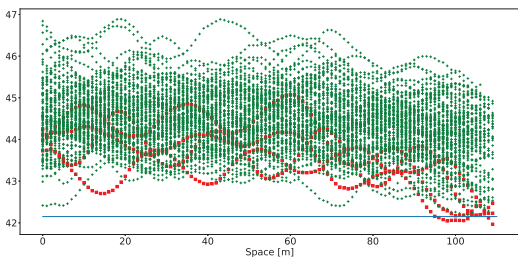In Figure 3, we report the trajectories sampled

Fig. 1.: Drift vs sections in χ_D for all the pipes. The pipes with $P_{2000,0.05} = 1$ are indicated with marker +, whereas the other pipes by marker □. The horizontal line represents threshold T_D.
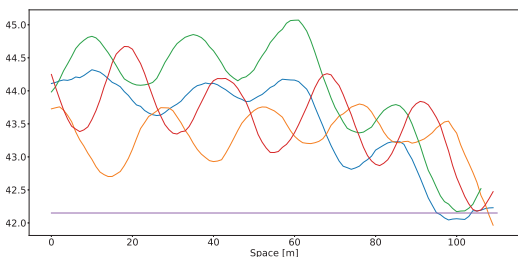

Fig. 2.: Drift of the pipes with $P_{2000,0.05} < 1$

from (Eq. 10) with the kernel γ_p^* for one of these

two pipes. From this, we can see that a few trajectories cross the threshold T_D.
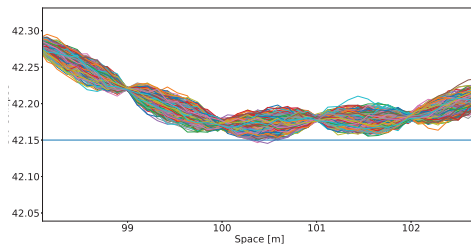

Fig. 3.: Sample trajectories: zoom on the threhold.

4.1. *Sensitivity analysis*

To evaluate the robustness of the proposed framework with respect to the set of kernels $\mathcal{K}_p$, we perform a sensitivity analysis by evaluating some accuracy performance metrics on the predictions obtained using different kernels on the same training and test data.

Namely, we consider (Rasmussen and Williams (2018)):

- a grid χ_D of $N_D = 99$ equally spaced points in $[1, 100]$.
- A set $\mathcal{S}$ of $|\mathcal{S}| = 7$ known 'target' kernels:
    - Radial Basis Function (RBF) (length scale=3)
    - Matérn 2.5 (length scale=7.0) times Periodic ($l = 2, P = 20$)
    - Rational Quadratic (length scale=2, $\alpha = 0.1$)
    - Matérn 1.5 (length scale=5)
    - Matérn 2.5 (length scale=10)
    - White Kernel (i.e., the points of the fields are independent on each other)
    - Matérn 0.5 (length scale=8)
- The set $\mathcal{K}_p$ of the candidate kernels considered in the previous Section.

For each kernel ks in $\mathcal{S}$, we sample $W = 40$ different realizations of $\mathbf{f}(\chi_D)$. Then, for each realization $w \in \{1, \dots, W\}$, we perform $3-$fold cross validation and fit the kernels belonging to set $\mathcal{K}_p$:

(1) We randomly divide $(\chi_D, \mathbf{f}(\chi_D))$ into three disjoint and mutually exhaustive sets of the same dimension, $(\chi_D^1, f(\chi_D^1))$, $(\chi_D^2, f(\chi_D^2)), (\chi_D^3, f(\chi_D^3))$.
(2) At each of the three cross-validation rounds and for each kl in $\mathcal{K}_p$:

(a) we estimate the $\boldsymbol{\theta}_{p,kl}^{MLE}$ parameters from the data of two of these sets (i.e, the training set of the considered cross-validation round) and compute the corresponding AIC.

(b) We evaluate the other performance metrics on the validation set.

For each combination of training and test kernel, we consider the average across all different realizations and cross-validation sets (i.e., $W \cdot 3$ different values) of:

- the binary indicator whether kernel kl yields the smallest AIC (i.e., it is the optimal one according to the kernel selection strategy reported in Section 3) among all candidates in $\mathcal{L}$.
- The 'precision' metric, which denotes the portion of points in the validation set where $\mathbf{f}(\chi_D)$ belongs to the 95% confidence interval by the considered kernel (the confidence interval is computed through Equation 10 and recalling that the normal distribution $\mathcal{N}(\mu, \sigma)$ has roughly 95% of its mass in $[\mu - 2 \cdot \sigma, \mu + 2 \cdot \sigma]$). Ideally, this value should be close to 95%.
- The 'mean bandwidth' metric, which denotes the average length of the confidence interval over all validation set points (the length of the confidence interval for the single point is $4 \cdot \sigma$). The smaller its value, the better the estimation, because there is less uncertainty in the prediction.

Table 2 reports for each 'target' kernel $ks \in \mathcal{S}$ (rows) the portion of times kernel $kl \in \mathcal{K}_p$ has the largest AIC value among all the candidates. Tables 3- 4 report for each combination of target kernel $kl \in \mathcal{K}_p$ (rows) and training kernel $ks \in \mathcal{S}$ the average value of the metrics 'precision' and 'mean bandwidth', respectively.

From the Tables, we can see that on the one hand with respect to the periodic 'target' kernel (i.e., Matérn 2.5 (length scale=7.0) times Periodic ($l = 2, P = 20$)), the non-periodic 'candidate' kernels never yield the smallest AIC value among all those belonging to $\mathcal{K}_p$ (Table 2, row 1). The fact that periodic 'candidate' kernels fit the periodic 'target' kernels better than the others is in accordance with the 'precision' value (Table 3, row 1), which is further away from the expected value of 0.95 with the non-periodic kernels (i.e., above 0.99 or below 0.9).

Furthermore, the 'mean bandwidth' metrics of the periodic training kernels is less than half of the corresponding values of the other training kernels (Tables 4, row 1).

Apart from the Matérn 2.5 kernel, the periodic training kernels have the smallest AIC value in non-periodic target kernels (Table 2, rows 2-7) in less than 20% of cases. Nonetheless, the values of the performance metrics are not dramatically different from those of the other kernels: even if the precision is different from 0.95 with respct to some of the non-periodic kernels, the 'mean bandwidth' of the periodic kernels is among the best of all $kl \in \mathcal{K}_p$. This is due to the fact that periodic and aperiodic kernels get closer as $P \to \infty$.

The problem with the periodic kernels tuned on non-periodic processes lies in that the larger number of useless parameters to set yields a more difficult parameter optimization. These observations lead to conclude that in the case study considered, the large frequency at which periodic kernels assume the largest AIC among all candidate values entails a non-negligible periodic behavior in the drift value of the available setof pipes.

Moreover, it is likely that the smallest AIC is taken on by a training kernel of the same type as the target kernel: 0.97 of the times the training RBF kernel has the smallest AIC for the target RBF kernel; similarly, 0.83 of the times the training Matérn 1.5 kernel has the smallest AIC for the target Matérn 1.5 kernel and 0.87 of the times the training Matérn 0.5 kernel has the smallest AIC for the target Matérn 0.5 kernel, Table 2). This confirms that the AIC value is a good criterion to select the optimal kernel: even if the 'mean bandwidth' of the candidate kernel of the same type as the target one is generally the smallest, this kernel does not differ so much from the other kernels in $\mathcal{K}_p$ in terms of the three metrics considered. Moreover, the combination of target and candidate RBF kernels has a poor accuracy (0.84).

The candidate white kernel in $\mathcal{K}_p$ is never selected as the optimal kernel, unless the target kernel is also the White kernel. Nonetheless, the precision metric always has a value of about 95%, because the confidence band is constant and corresponds to the total variability of the considered field (i.e., the mean and max bandwidth range from 2 to 20 times the band value of the optimal candidate kernel). When the white kernel is the target kernel, the candidate kernel is selected randomly in $\mathcal{K}_p$. Nonetheless, the optimal parameters are set so that the values of the 'precision' and 'mean bandwidth' are the same across all candidate kernels (i.e., the 'precision' is always close to 0.95 and the mean bandwidth is $\simeq 2$). Notice that the precision of the periodic kernels against the target white kernel is slightly smaller than those of the other kernels, due to the more difficult parameter optimization issue.

5. Conclusions

In this work, we have used Gaussian fields to estimate the pipe drift conformance probability based on the geometrical data relevant to a single pipe. Our framework relies on the selection of the best

Proceedings of the 30th European Safety and Reliability Conference and the 15th Probabilistic Safety Assessment and Management Conference

2732

Table 2.: Percentage of times in which the combination of each kernel has the smallest AIC value.

	Periodic times Matérn 0.5	Periodic times Matérn 1.5	Periodic times Matérn 1.5 + Periodic times Matérn 0.5
Matérn 2.5 (length scale=7.0) times Periodic ($l=2, P=20$)	0.11	0.85	0.04
RBF (length scale=3)	0	0.033	0
Rational Quadratic (length scale=2, $\alpha=0.1$)	0.083	0.025	0.0083
Matérn 1.5 (length scale=5)	0.075	0.05	0.042
Matérn 2.5 (length scale=10)	0	0.86	0.092
White Kernel	0.12	0.05	0.0083
Matérn 0.5 (length scale=8)	0.033	0.05	0.0083

	Matérn 1.5	Matérn 0.5	RBF	White Kernel
Matérn 2.5 (length scale=7.0) times Periodic ($l=2, P=20$)	0	0	0	0
RBF (length scale=3)	0	0	0.97	0
Rational Quadratic (length scale=2, $\alpha=0.1$)	0.38	0.47	0.033	0
Matérn 1.5 (length scale=5)	0.83	0	0	0
Matérn 2.5 (length scale=10)	0.05	0	0	0
White Kernel	0.35	0.23	0.22	0.025
Matérn 0.5 (length scale=8)	0.042	0.87	0	0

Table 3.: 'Precision' of the different combinations of target (rows) and training (columns) kernels.

	Periodic times Matérn 0.5	Periodic times Matérn 1.5	Periodic times Matérn 1.5 + Periodic times Matérn 0.5
Matérn 2.5 (length scale=7.0) times Periodic ($l=2, P=20$)	0.93	0.96	0.93
RBF (length scale=3)	0.99	0.82	0.84
Rational Quadratic (length scale=2, $\alpha=0.1$)	0.93	0.91	0.90
Matérn 1.5 (length scale=5)	0.93	0.93	0.89
Matérn 2.5 (length scale=10)	0.94	0.96	0.95
White Kernel	0.92	0.92	0.90
Matérn 0.5 (length scale=8)	0.94	0.91	0.91

	Matérn 1.5	Matérn 0.5	RBF	White Kernel
Matérn 2.5 (length scale=7.0) times Periodic ($l=2, P=20$)	0.99	0.995	0.80	0.96
RBF (length scale=3)	0.995	0.99	0.84	0.95
Rational Quadratic (length scale=2, $\alpha=0.1$)	0.93	0.96	0.91	0.95
Matérn 1.5 (length scale=5)	0.95	0.99	0.87	0.95
Matérn 2.5 (length scale=10)	0.99	0.997	0.76	0.96
White Kernel	0.95	0.95	0.95	0.95
Matérn 0.5 (length scale=8)	0.93	0.95	0.90	0.95

fitting kernel among a set of candidates through AIC and the computation of the probability that the drift value is above the critical threshold in a fine grid of points amid the measurement sections. The application of the presented framework to a case study has shown that even if all points in the measurement sections have a drift value above the critical threshold, this s not sufficinet to accept the pipe. We have also assessed the robustness of our kernel selection methodology through a sensitivity analysis with respect to different known target kernels.

References

Adler, R. (1981). *The Geometry of Random Fields*. Chichester: Wiley.

Adler, R. (2000). On excursion sets, tube formulas and maxima of random fields. *The Annals of Applied Probability 10*(1), 1–74.

Adler, R. and J. Taylor (2007). *Random Fields and Geometry*. Springer Monographs in Mathemat-

Table 4.: Mean bandwidth of the different combinations of target (rows) and training (columns) kernels.

	Periodic times Matérn 0.5	Periodic times Matérn 1.5	Periodic times Matérn 1.5 + Periodic times Matérn 0.5	
Matérn 2.5 (length scale=7.0) times Periodic ($l = 2, P = 20$)	0.078	0.078	0.075	
RBF (length scale=3)	0.06	0.028	0.029	
Rational Quadratic (length scale=2, $\alpha = 0.1$)	0.89	0.88	0.84	
Matérn 1.5 (length scale=5)	0.57	0.54	0.52	
Matérn 2.5 (length scale=10)	0.079	0.066	0.064	
White Kernel	1.91	1.92	1.84	
Matérn 0.5 (length scale=8)	1.32	1.32	1.27	
	Matérn 1.5	Matérn 0.5	RBF	White Kernel
Matérn 2.5 (length scale=7.0) times Periodic ($l = 2, P = 20$)	0.15	0.45	0.16	1.85
RBF (length scale=3)	0.48	1.36	0.029	4.18
Rational Quadratic (length scale=2, $\alpha = 0.1$)	0.90	0.97	0.98	1.87
Matérn 1.5 (length scale=5)	0.56	0.96	0.77	3.04
Matérn 2.5 (length scale=10)	0.10	0.50	0.21	3.5
White Kernel	1.99	1.99	1.99	2
Matérn 0.5 (length scale=8)	1.36	1.38	1.61	3.09

ics. New York: Springer.

Akaike, H. (1974, December). A new look at the statistical model identification. *IEEE Transactions on Automatic Control 19*(6), 716–723.

API (1994). Bulletin on formulas and calculations for casing, tubing, drill pipe and line properties. *API Bulletin 5C3, 6th ed.*.

Azzimonti, D., J. Bect, C. Chevalier, and D. Ginsbourger (2016). Quantifying uncertainties on excursion sets under a gaussian random field prior. *SIAM/ASA Journal on Uncertainty Quantification 4*(1), 850–874.

Baker, J. W. and M. H. Faber (2007). Sampling strategies to detect threshold excursions in random fields. *Reliability and Optimization of Structural Systems: Assessment, Design, and Life-Cycle Performance*, 53.

Chevalier, C., J. Bect, D. Ginsbourger, E. Vazquez, V. Picheny, and Y. Richet (2014). Fast parallel kriging-based stepwise uncertainty reduction with application to the identification of an excursion set. *Technometrics 56*(4), 455–465.

Crooks, E. (29 Feb. 2016). How can the oil industry cut costs. *Financial Times*.

Duvenaud, D., J. R. Lloyd, R. Grosse, J. B. Tenenbaum, and Z. Ghahramani (2013). Structure discovery in nonparametric regression through compositional kernel search.

Hovem, L. (2019). The outlook for the oil and gas industry in 2019. *DNV GL's Industry Outlook report*.

ISO/IEC-GUIDE:98-4 (2012). Uncertainty of measurement - part 4: Role of measurement uncertainty in conformity assessment.

ISO/TR-10400 (2007). Petroleum and natural gas industries-formula and calculation for casing, tubing, drill pipe and line pipe properties.

Pinciroli, L., M. Compare, E. Zio, G. Almeida, and P. Filgueiras (2019). Gaussian fields for predicting the drift of pipes for deep-water applications. *Submitted for pubblication*.

Rasmussen, C. E. and C. K. I. Williams (2018). Gaussian processes for machine learning.

Stone, M. (1979). Comments on model selection criteria of akaike and schwarz. *Journal of the Royal Statistical Society. Series B (Methodological) 41*(2), 276–278.